First results of axion dark matter search with DANCE

Yuka Oshima,[1,*] Hiroki Fujimoto,[1] Jun'ya Kume,[1,2] Soichiro Morisaki,[3] Koji Nagano,[4] Tomohiro Fujita,[5,2] Ippei Obata,[6] Atsushi Nishizawa,[2] Yuta Michimura,[7,2,8] and Masaki Ando[1,2]

[1]*Department of Physics, University of Tokyo, Bunkyo, Tokyo 113-0033, Japan*
[2]*Research Center for the Early Universe (RESCEU), University of Tokyo, Bunkyo, Tokyo 113-0033, Japan*
[3]*Institute for Cosmic Ray Research, University of Tokyo, Kashiwa, Chiba 277-8582, Japan*
[4]*Institute of Space and Astronautical Science, Japan Aerospace Exploration Agency, Sagamihara, Kanagawa 252-5210, Japan*
[5]*Waseda Institute for Advanced Study, Waseda University, Shinjuku, Tokyo 169-8050, Japan*
[6]*Kavli Institute for the Physics and Mathematics of the Universe (WPI), University of Tokyo, Kashiwa, Chiba 277-8583, Japan*
[7]*LIGO Laboratory, California Institute of Technology, Pasadena, California 91125, USA*
[8]*PRESTO, Japan Science and Technology Agency (JST), Kawaguchi, Saitama 332-0012, Japan*

(Received 18 March 2023; revised 6 September 2023; accepted 14 September 2023; published 10 October 2023; corrected 10 May 2024)

Axions are one of the well-motivated candidates for dark matter, originally proposed to solve the strong *CP* problem in particle physics. Dark matter Axion search with riNg Cavity Experiment (DANCE) is a new experimental project to broadly search for axion dark matter in the mass range of 10^{-17} eV $< m_a < 10^{-11}$ eV. We aim to detect the rotational oscillation of linearly polarized light caused by the axion-photon coupling with a bow-tie cavity. The first results of the prototype experiment, DANCE Act-1, are reported from a 24-hour observation. We found no evidence for axions and set 95% confidence level upper limit on the axion-photon coupling $g_{a\gamma\gamma} \lesssim 8 \times 10^{-4}$ GeV^{-1} in 10^{-14} eV $< m_a < 10^{-13}$ eV. Although the bound did not exceed the current best limits, this optical cavity experiment is the first demonstration of polarization-based axion dark matter search without any external magnetic field.

DOI: 10.1103/PhysRevD.108.072005

I. INTRODUCTION

Axions are hypothetical particles generated from a pseudoscalar field originally proposed to solve the strong *CP* problem in quantum chromodynamics (QCD) [1]. This idea is generally called the "QCD axion." Moreover, string theory predicts a plenitude of axionlike particles (ALPs) [2]. QCD axions and ALPs are one of the well-motivated candidates for dark matter (DM) because of their small masses and tiny interactions with matter sectors, and could behave like a nonrelativistic classical wave field in the history of the universe [3–6]. Hereafter in this article, we collectively call them "axions."

The conventional way of searching for axions is to detect a phenomenon where axions convert into photons under an external magnetic field and vice versa, known as the Primakoff effect [7–9]. Astronomical observations are useful to probe the axion-photon conversion in the (extra) galactic magnetic fields, but no strong evidence has been found [10,11]. CERN Axion Solar Telescope (CAST) looked for axions thermally produced in the Sun with a strong dipole magnet and set the current limit on the axion-photon coupling [12]. Some new projects with toroidal coils probed a tiny oscillatory magnetic field caused by axion DM and achieved the competitive limits to CAST [13,14].

Recently, new experimental approaches to search for axions were proposed that do not need any strong magnetic field but use optical cavities instead [15–24]. These methods aim to detect the phase velocity difference between left- and right-handed circular polarizations caused by a small coupling between axions and photons [25,26]. Laser interferometers are good at probing frequencies of $\lesssim$100 kHz and thus they have a good sensitivity in the corresponding axion mass region of $m_a \lesssim 10^{-10}$ eV. A key point in these techniques is how to cancel the polarization flipping due to the reflection on mirrors in order to accentuate the axion effect. One suggestion is to use a Mach-Zehnder interferometer with two cavities and a polarizing beam splitter [15], and another would be to use a Michelson interferometer with quarter-wave plates inside two arm cavities [16]. The

*yuka.oshima@phys.s.u-tokyo.ac.jp

authors of Ref. [17] came up with an idea to use a bow-tie ring cavity: Dark matter Axion search with riNg Cavity Experiment (DANCE) [22–24]. A bow-tie cavity is used to enhance the axion signal without any optics inside the cavity, which prevents optical elements from lowering the finesse of the cavity. The methods of injecting linearly polarized beam and tuning mirror angles [18], and applying squeezed states of light [19] were also proposed to improve the sensitivity over a wide range of axion masses.

In this work, we demonstrated the prototype experiment, DANCE Act-1, and obtained the upper limit on the axion-photon coupling from a 24-hour observation. This optical cavity experiment is the first demonstration of polarization-based axion DM search without any external magnetic field. This article is organized as follows. Section II gives a brief summary of the rotational oscillation of optical linear polarization caused by axion DM and an expected sensitivity obtained by axion signal amplification using a bow-tie cavity. Section III reports the experimental setup, its performance, and data acquisition. In Sec. IV the data analysis and results are described. Section V discusses the causes of sensitivity degradation. Finally, we conclude this work in Sec. VI.

II. PRINCIPLE AND SENSITIVITY

In this section, we briefly revisit the dynamics of the axion field, calculate its oscillation amplitude, and derive the sensitivity of our experiment to the axion-photon coupling. We set the natural unit $\hbar = c = 1$ unless otherwise noted.

Axions couple to photons through the Chern-Simons interaction,

$$\begin{aligned}\mathcal{L} &\supset \frac{g_{a\gamma\gamma}}{4} a(t) F_{\mu\nu}\tilde{F}^{\mu\nu} \\ &= g_{a\gamma\gamma}\dot{a}(t)\epsilon_{ijk}A_i\partial_j A_k + (\text{total derivative}),\end{aligned} \tag{1}$$

where dot denotes the time derivative, $g_{a\gamma\gamma}$ is the axion-photon coupling constant, $a(t)$ is the axion field value, A_μ is the vector potential, and $F_{\mu\nu} \equiv \partial_\mu A_\nu - \partial_\nu A_\mu$. $\tilde{F}^{\mu\nu} \equiv \epsilon^{\mu\nu\rho\sigma}F_{\rho\sigma}/2$ is its Hodge dual defined with the Levi-Civita antisymmetric tensor $\epsilon^{\mu\nu\rho\sigma}$. We impose the temporal gauge $A_0 = 0$ and the Coulomb gauge $\nabla \cdot \boldsymbol{A} = 0$. Then the equation of motion can be written as

$$\ddot{A}_i - \nabla^2 A_i + g_{a\gamma\gamma}\dot{a}(t)\epsilon_{ijk}\partial_j A_k = 0. \tag{2}$$

We decompose A_i into two circular polarization modes in the Fourier space

$$A_i(t,\boldsymbol{x}) = \sum_{\alpha=\mathrm{L,R}} \int_{-\infty}^{\infty} \frac{\mathrm{d}^3k}{(2\pi)^3} A_\alpha(t,\boldsymbol{k}) e_{\alpha,i}(\hat{\boldsymbol{k}}) e^{i\boldsymbol{k}\cdot\boldsymbol{x}}, \tag{3}$$

where the index α of L, R represents left- and right-handed photons, $\boldsymbol{k}$ is the wave number vector, and $e_{\alpha,i}(\hat{\boldsymbol{k}})$ is the circular polarization vector. By substituting Eq. (3) into Eq. (2), we obtain the angular frequencies

$$\omega_{\mathrm{L/R}}^2 = k^2\left(1 \mp \frac{g_{a\gamma\gamma}\dot{a}(t)}{k}\right) \tag{4}$$

and the phase velocities

$$c_{\mathrm{L/R}} \equiv \frac{\omega_{\mathrm{L/R}}}{k} \simeq 1 \mp \frac{g_{a\gamma\gamma}\dot{a}(t)}{2k}. \tag{5}$$

The axion field is expressed by a periodic oscillation,

$$a(t) = a_0 \cos(m_a t + \delta_\tau(t)), \tag{6}$$

where the axion mass m_a represents the angular frequency. The frequency of axion mass can be written as $f_a = m_a/(2\pi) \simeq 2.4\ \mathrm{Hz}(m_a/10^{-14}\ \mathrm{eV})$. The phase factor $\delta_\tau(t)$ can be regarded as a constant value within the constant timescale of axion DM, τ, expressed as $\tau = 2\pi/(m_a v_a^2)$, where $v_a \sim 10^{-3}$ is the DM velocity near the Sun. Plugging Eq. (6) into Eq. (5), we obtain

$$c_{\mathrm{L/R}} = 1 \pm \delta c(t), \tag{7}$$

$$\delta c(t) \equiv \frac{g_{a\gamma\gamma}\sqrt{2\rho_a}}{2k}\sin(m_a t + \delta_\tau(t)), \tag{8}$$

where $\rho_a = m_a^2 a_0^2/2 = 0.4\ \mathrm{GeV/cm^3}$ is the DM energy density in the Sun.

This phase velocity difference causes linearly polarized light to rotate [25,26]. Let $\boldsymbol{E}(z=0,t) = E_0 e^{i\omega_0 t}\boldsymbol{e}_\mathrm{s}$ defined as the s-polarized injection beam propagating along the z axis with angular frequency ω_0 from $z = 0$. The electric field at $z = l$ can be written as

$$\boldsymbol{E}(z=l,t) = E_0 e^{i\omega t}(\boldsymbol{e}_\mathrm{s}\boldsymbol{e}_\mathrm{p})\begin{pmatrix} 1 \\ -\delta\theta(l,t)\end{pmatrix}, \tag{9}$$

$$\begin{aligned}\delta\theta(l,t) &\equiv k_0\int_{t-l}^{t}\delta c(t)\mathrm{d}t \\ &= \frac{g_{a\gamma\gamma}\sqrt{2\rho_a}}{m_a}\sin\left(m_a\left(t-\frac{l}{2}\right)+\delta_\tau\right)\sin\left(m_a\frac{l}{2}\right),\end{aligned} \tag{10}$$

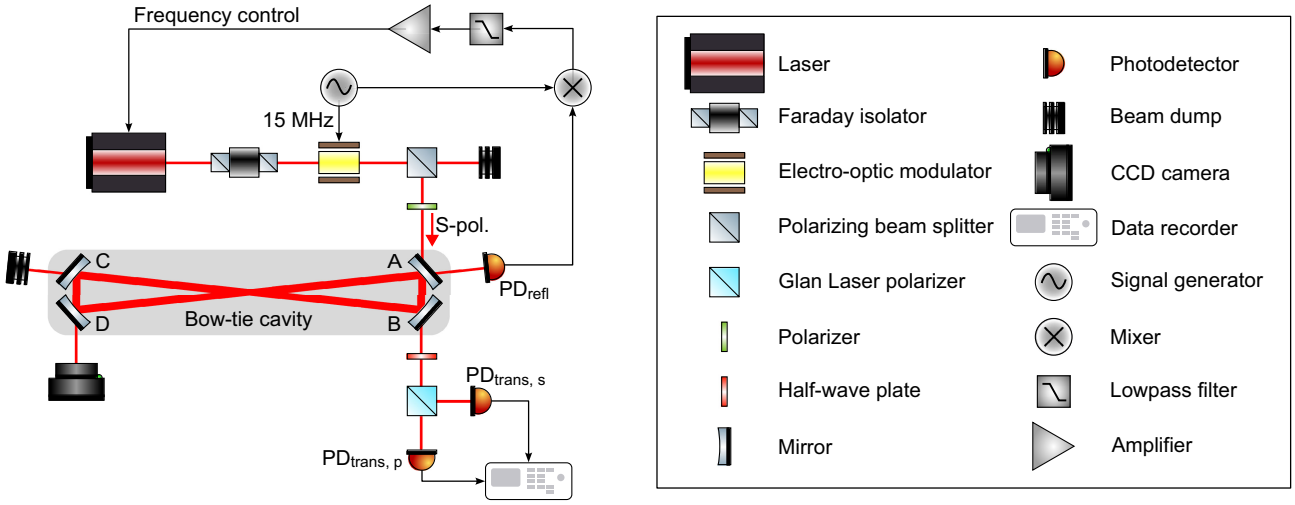

FIG. 1. The schematic of an experimental setup for DANCE Act-1.

when assuming $\delta\theta(l,t) \ll 1$. Here $k_0 = \omega_0/c$ is the wave number without axions. The plane of linearly polarized light at $z = 0$ rotates by $-\delta\theta(l,t)$ at $z = l$. Small p-polarized sidebands are generated from s-polarized carrier beam, and vice versa, in the presence of axions [18].

The sensitivity of DANCE Act-1 can be calculated using a method described in Ref. [27]. We assume that s-polarized light is injected into a bow-tie ring cavity, with an electric field of $\boldsymbol{E}_{\rm in}(t) = E_0 e^{i\omega_0 t}\boldsymbol{e}_{\rm s}$. The schematic of an experimental setup for DANCE Act-1 is shown in Fig. 1 and the symbols of the parameters are summarized in Table I. Under the assumption that mirrors do not have any optical losses, the electric field of transmitted light is estimated as

$$\boldsymbol{E}_{\rm trans}(t) = \frac{(1-r_{1\rm s}^2)e^{-ik_0 l_1}}{(1-r_{1\rm s}^2 r_{2\rm s}^2)e^{-ik_0(2l_1+2l_2)}} \times E_0 e^{i\omega_0 t}(\boldsymbol{e}_{\rm s}\boldsymbol{e}_{\rm p})\begin{pmatrix}1\\ -\delta\phi(t)\end{pmatrix}, \tag{11}$$

$$\delta\phi(t) \equiv \int_{-\infty}^{\infty}\frac{{\rm d}\omega}{2\pi}\tilde{\delta c}(\omega)e^{i\omega t}H_a(\omega), \tag{12}$$

where $\delta\phi(t)$ is a polarization rotation angle of transmitted light. $H_a(\omega)$ is a transfer function from $\delta c(t)$ to $\delta\phi(t)$:

TABLE I. Summary of the parameters for DANCE Act-1. The difference of the reflective phase shift between s- and p-polarizations is written in the conversion to the FSR of the cavity [$\delta\nu$ = phase shift[rad]$/(2\pi) \times c/(2l_1 + 2l_2)$]. The parameters of the final design are listed to show the ideal sensitivity (plotted as the green curve in Fig. 6).

Parameter	Symbol	Final design	This experiment
Injected laser power	$P_{\rm in}$	1 W	242(12) mW
Transmitted laser power	$P_{\rm trans}$	1 W	153(8) mW
Distance between A and D, B and C	l_1	45 cm	45 cm*
Distance between A and B, C and D	l_2	4.7 cm	4.7 cm*
Power reflectivity of s-pol. (A and B)	$\lvert r_{1\rm s}\rvert^2$	99.9%	99.90(2)%*
Power reflectivity of s-pol. (C and D)	$\lvert r_{2\rm s}\rvert^2$	100%	$>$ 99.99%*
Power reflectivity of p-pol. (A and B)	$\lvert r_{1\rm p}\rvert^2$	99.9%	98.42(2)%
Power reflectivity of p-pol. (C and D)	$\lvert r_{2\rm p}\rvert^2$	100%	99.95(1)%
Finesse of s-pol. (carrier)	$\mathcal{F}_{\rm s}$	3×10^3	$2.85(5) \times 10^3$
Finesse of p-pol. (signal sidebands)	$\mathcal{F}_{\rm p}$	3×10^3	195(3)
Total difference of the reflective phase shift between s- and p-pol.	$\delta\nu_{\rm total}$	0 Hz	2.52(2) MHz
Difference of the reflective phase shift between s- and p-pol. (A and B)	$\delta\nu_1$	0 Hz	−0.55(97) MHz
Difference of the reflective phase shift between s- and p-pol. (C and D)	$\delta\nu_2$	0 Hz	2.08(99) MHz

The values with stars are specifications, and the others are measured values

$$H_a(\omega) \equiv k_0 \sqrt{\frac{1-|r_{1p}|^2}{1-|r_{1s}|^2}} \frac{1}{i\omega(1-r_{1p}^2 r_{2p}^2 e^{-i\omega(2l_1+2l_2)})} \Big[(1-e^{-i\omega l_2})\Big(r_{1s}r_{2s}r_{1p}r_{2p}e^{-i\omega l_1} + r_{1p}^2 r_{2p}^2 e^{-i\omega(2l_1+l_2)}\Big) - (1-e^{-i\omega l_1})\Big(r_{1s}r_{2s}^2 r_{1p} + r_{1s}r_{1p}r_{2p}^2 e^{-i\omega(l_1+l_2)}\Big)\Big]. \tag{13}$$

The optical path length can be effectively increased using an optical cavity and axion signal is accumulated in the cavity. We set the reflectivity of s-polarization, r_{1s} and r_{2s}, as real numbers, whereas that of p-polarization, r_{1p} and r_{2p}, are complex numbers and contain the information about the difference of the reflective phase shift between s- and p-polarizations. For example, $r_{1p} = |r_{1p}| \exp[-2\pi i(2l_1 + 2l_2)\delta\nu_1/c]$ where $\delta\nu_1$ is the reflective phase difference converted to the free spectral range (FSR) of a bow-tie cavity. $c/(2l_1 + 2l_2)$ represents the FSR and its value in DANCE Act-1 is 302 MHz.

Figure 2 represents the response function $|H_a(m_a)|$. When $\delta\nu_1 = \delta\nu_2 = 0$, the sensitivity in the low mass region ($m_a \lesssim 10^{-12}$ eV) will be the highest. When $\delta\nu_1 \neq 0$ or $\delta\nu_2 \neq 0$, the sensitivity in the low mass region will be lower. However, the sensitivity is enhanced at the mass corresponding to the total reflective phase difference between s- and p-polarizations $\delta\nu_{\rm total}$ since signal sideband is enhanced in a bow-tie cavity.

The sensitivity of DANCE depends on the method of detection. The detailed setup of this work is described in Sec. III. The fundamental noise source of DANCE would be quantum shot noise and the potential sensitivity limited by shot noise is roughly estimated as

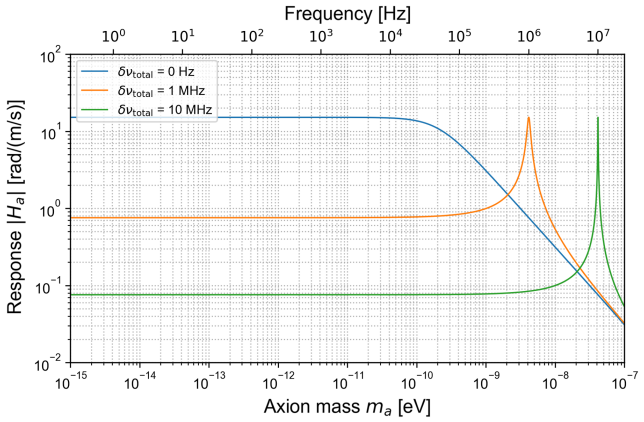

FIG. 2. The response function $|H_a|$. The blue line shows the function $|H_a|$ for $\delta\nu_1 = \delta\nu_2 = 0$ Hz ($\delta\nu_{\rm total} = 0$ Hz), the orange line for $\delta\nu_1 = \delta\nu_2 = 0.25$ MHz ($\delta\nu_{\rm total} = 1$ MHz), and the green line for $\delta\nu_1 = \delta\nu_2 = 2.5$ MHz ($\delta\nu_{\rm total} = 10$ MHz). The other parameters are the same as the final design of DANCE Act-1 as shown in Table I.

$$g_{a\gamma\gamma} \geq \begin{cases} 227\ \mathrm{GeV}^{-1} \frac{|1-r_{1s}^2 r_{2s}^2|}{|1-r_{1s}^2|} \frac{\mathrm{eV}^{-1}}{|H_a'(m_a)|/k_0} \\ \times \sqrt{\frac{\mathrm{GeV/cm^3}}{\rho_a} \frac{\mathrm{W}}{P_{\rm in}} \frac{\mu\mathrm{m}}{\lambda_0} \frac{\mathrm{s}}{T_{\rm obs}}} & (T_{\rm obs} \lesssim \tau), \\ 227\ \mathrm{GeV}^{-1} \frac{|1-r_{1s}^2 r_{2s}^2|}{|1-r_{1s}^2|} \frac{\mathrm{eV}^{-1}}{|H_a'(m_a)|/k_0} \\ \times \sqrt{\frac{\mathrm{GeV/cm^3}}{\rho_a} \frac{\mathrm{W}}{P_{\rm in}} \frac{\mu\mathrm{m}}{\lambda_0} \frac{\mathrm{s}}{(T_{\rm obs}\tau)^{1/2}}} & (T_{\rm obs} \gtrsim \tau), \end{cases} \tag{14}$$

$$|H_a'(m_a)| \equiv \frac{1}{2}\{(\mathrm{Re}[H_a(m_a) + H_a(-m_a)])^2 + (\mathrm{Im}[H_a(m_a) - H_a(-m_a)])^2\}^{\frac{1}{2}}, \tag{15}$$

where λ_0 is a laser wavelength and $|H_a'(m_a)|$ is a signal amplification factor by a bow-tie cavity. We assume that we can observe axions when ratio between axion signal and shot noise ≥ 1. The sensitivity improves as the measurement time increases, with the factor of $T_{\rm obs}^{1/2}$ as long as the axion oscillation is coherent for $T_{\rm obs} \lesssim \tau$, where τ is the coherent timescale of axion DM. When the measurement time becomes longer than this coherence time $T_{\rm obs} \gtrsim \tau$, the proportionality of the sensitivity with the measurement time changes to $(T_{\rm obs}\tau)^{1/4}$. This different proportionality is owing to the stochasticity of the amplitude of axion field [28], which will be discussed in Sec. IV.

Even using conservative parameters listed in Table I, DANCE Act-1 can exceed the CAST limit (see the green curve in Fig. 6). If we use more optimistic parameters, with a round-trip length of 10 m, finesse of 10^6, and input laser power of 100 W, we can reach $g_{a\gamma\gamma} < 3 \times 10^{-16}$ GeV^{-1} for $m_a < 10^{-16}$ eV [17] and improve the sensitivity broadly by several orders of magnitude compared to the best upper limits at present.

III. EXPERIMENT

In this section, the experimental setup, its performance, and data acquisition are reported.

A. Setup and performance

Figure 1 shows the experimental setup of DANCE Act-1. We used a Nd:YAG laser, Mephisto 500 NE, with a wavelength of 1064 nm. The s-polarized beam was injected into a bow-tie cavity. We put a polarizing beam splitter as well as a polarizer in front of the cavity to have linearly

polarized light injected into the cavity. Our bow-tie cavity was constructed from four mirrors A-D rigidly fixed on a spacer made of aluminum.

We aim to probe the axion signal by taking the interference between a carrier beam (s-polarization in this work) and signal sidebands (p-polarization) in the direction of amplitude quadrature [18]. Polarization of transmitted light was rotated with a half-wave plate to introduce some p-polarized reference signal which has the same frequency as a carrier beam, and then split into s- and p-polarizations with a Glan Laser polarizer. The amplitudes of s- and p-polarizations were monitored with photodetectors $\mathrm{PD}_{\mathrm{trans,s}}$ and $\mathrm{PD}_{\mathrm{trans,p}}$ and saved with a data recorder for two weeks.

The laser frequency was locked to the resonance of TEM00 mode by obtaining the error signal for the laser frequency control with the Pound-Drever-Hall method [29]. Spatial mode is confirmed to be TEM00 using a CCD camera. To improve the lock duration time, the double-loop feedback control system and the automated cavity locking system were developed [30]. Feedback signal above ~30 Hz was sent into the laser fast port (piezo actuator), and feedback signal under ~30 Hz was sent into the laser slow port (temperature actuator). To implement this system, we used SEAGULL mini as a digital signal processor, and also as a lowpass filter for the low frequency control loop. A digital signal processor monitored the output of $\mathrm{PD}_{\mathrm{trans,s}}$ and identified whether the cavity was locked or unlocked. When the cavity was unlocked, signal into the laser slow port was swept until the cavity is locked again.

l_1 was designed to be around 10 times longer than l_2 to enhance the rotational oscillation of s-polarization by preventing the linear polarization from inverting when reflecting on mirrors. We specified only $|r_{1s}|^2$ and $|r_{2s}|^2$ when we ordered custom-made mirrors A-D because it is difficult to control the reflective phase shift and to satisfy our requirements. All the four mirrors were concave mirrors with a radius of curvature of 1 m. Beam diameter on the mirrors was ~800 μm. Incident angles at all the four mirrors were 42 deg.

$\mathcal{F}_s$, $\mathcal{F}_p$, and $\delta\nu_{\mathrm{total}}$ were measured by sweeping cavity resonances. $\mathcal{F}_s$ was consistent with the specified reflectivity $|r_{1s}|^2$ and $|r_{2s}|^2$ and we could achieve a high finesse. $\delta\nu_{\mathrm{total}}$ was nonzero because each polarization obtains a different phase shift from mirror-coating layers when reflecting at oblique incident angles. Note that $\delta\nu_{\mathrm{total}}$ drifted from 2.52(2) MHz to 0.50(2) MHz in the two-week observation. We obtained $\delta\nu_1$ and $\delta\nu_2$ separately for data analysis. We used mirrors with different coating layers to build the cavity and measured $\delta\nu_{\mathrm{total}}$ with various mirror combinations. Assuming that mirrors with the same coating layers have the same phase shift, we determined $\delta\nu_1$ and $\delta\nu_2$.

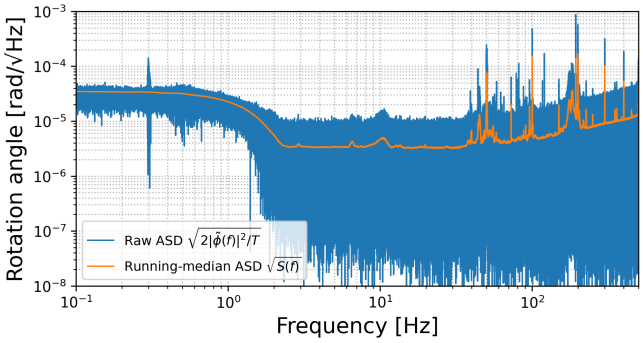

FIG. 3. The one-sided ASD of the rotation angle of linear polarization.

B. Data acquisition

The time series data of s- and p-polarizations, $P_s(t)$ and $P_p(t)$, was observed with a sampling rate of 1 kHz for 1,004,400 seconds in May 18–30, 2021. We analyzed two sets of continuous 86,400-second (24-hour) data on May 18 and 19 because the first two days were the stretch of time with the most stable lock. One set was used to set the upper limit and the other was used to veto candidate peaks.

We calibrated the output of photodetectors $P_s(t)$ and $P_p(t)$ to the rotation angle of linear polarization $\phi(t)$ by

$$\phi(t) = \sqrt{\frac{P_p(t)}{P_s(t) + P_p(t)}} - 2\theta_{\mathrm{HWP}}, \tag{16}$$

where θ_{HWP} is the rotation angle of the half-wave plate with respect to the s-polarized light at the detection port. We do not need to measure θ_{HWP} because it is a constant parameter and we focus on oscillational amplitudes. The one-sided amplitude spectral density (ASD) of the observed rotation angle of linear polarization is plotted in Fig. 3. We reached 3.4×10^{-6} rad$/\sqrt{\mathrm{Hz}}$ at 5 Hz.

IV. DATA ANALYSIS

In this section, we describe our analysis of the data to place upper limit on the axion-photon coupling.

A. Detection statistics

The signal is expected to have a bandwidth of $\sim f_a v_{\mathrm{vir}}^2$, where v_{vir} is the virial velocity of our Galaxy [31]. Thus, for axion mass value m_a, we define the following signal-to-noise ratio (SNR) as a detection statistic:

$$\rho \equiv \sum_{f_a \le f_n \le f_a(1+\kappa^2 v_{\mathrm{vir}}^2)} \frac{4|\tilde{\phi}(f_n)|^2}{TS(f_n)}, \tag{17}$$

where T is the duration of the data segment, f_n is the discretized frequency bin, κ is a constant of order unity, $\tilde{\phi}(f)$ represents the Fourier-transformation of $\phi(t)$, and

$S(f)$ is the one-sided noise power spectral density. Note that in the absence of the signal $\delta\phi(t)$, this corresponds to the orange curve in Fig. 3. Raw ASD is also plotted in Fig. 3. We adopt $v_{\rm vir} = 220$ km/s [32,33], and $\kappa = 3.17$ to guarantee that the fractional loss of signal is less than 99% assuming the standard halo model of DM velocity distribution. Here $S(f_n)$ is evaluated by the running median from $\sim 8,600$ neighboring frequency bins in order to smear out the effect of DM signal localized in the narrow band.

The detection threshold of ρ is determined under the assumption that the instrumental noise is a stationary Gaussian process. In the absence of a signal, ρ follows a χ^2 distribution with $2N_{\rm bin}$ degrees of freedom, where $N_{\rm bin}$ denotes the number of frequency bins involved in the sum of Eq. (17). We chose the threshold to be the 95% percentile of that distribution. For each case where the measured value of ρ exceeds this threshold, we performed the veto analysis as explained below.

The upper bound on the signal amplitude is calculated in the frequentist method introduced by Ref. [28]. Because the axion field is superposition of particle waves with random phase, its amplitude randomly fluctuates. The analysis method proposed by the previous work takes into account this random axion amplitude. Let $\delta\phi^{(\rm upp)}(m_a)$ denote the upper bound on the root-mean-square (RMS) of $\delta\phi(t)$ in Eq. (12) for axion mass value m_a. At the confidence level β, it is calculated by the following equation,

$$1-\beta = \int_0^{\rho_{\rm mea}(m_a)} {\rm d}\rho\, \mathcal{L}(\rho|\delta\phi^{(\rm upp)}(m_a)), \tag{18}$$

where $\rho_{\rm mea}(m_a)$ is the measured value of ρ, and $\mathcal{L}(\rho|\delta\phi)$ is the likelihood of observing detection statistics ρ conditioned on signal with RMS $\delta\phi$. Note again that the effect of randomness in the axion DM amplitude mentioned above is included in the likelihood function derived in Ref. [28]. The interested readers can find the concrete expressions of this likelihood in the Appendix. We chose $\beta = 0.95$ for the numerical calculation of the upper bound. This upper bound on the rotation angle can be converted into that on the axion-photon coupling through the following relation:

$$\begin{aligned} g_{a\gamma\gamma}(m_a) &= \frac{2k_0\delta\phi^{(\rm upp)}(m_a)}{\sqrt{2\rho_a}|H_a'(m_a)|} \\ &= 5.10\times 10^{11}\ {\rm GeV}^{-1}\frac{{\rm eV}^{-1}}{|H_a'(m_a)|/k_0} \\ &\quad\times\sqrt{\frac{{\rm GeV/cm}^3}{\rho_a}}\delta\phi^{(\rm upp)}(m_a). \end{aligned} \tag{19}$$

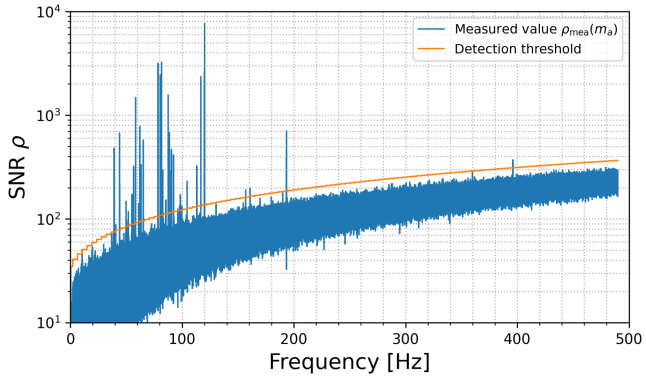

FIG. 4. SNR ρ of axion DM signal for each frequency f_a. The blue line shows the measured value $\rho_{\rm mea}(m_a)$ and the orange line represents the detection threshold.

B. Results

After passing the first 24-hour dataset through our pipeline for calculating $\rho_{\rm mea}(m_a)$, 556 points exceeded the detection threshold of ρ out of a total of 1,776,390 points in 0.1–490 Hz as shown in Fig. 4. We conducted the following two veto procedures: the persistence veto and the line width veto.

An axion signal should have the same frequency in two segments of data with the accuracy of $\Delta\omega/\omega \sim 10^{-6}$ [31]. We rejected the points that did not match the second set of data with 6 significant digits accuracy. This persistence veto reduced the number of candidate points to 257.

Since the expected line width of the galactic DM is $\Delta\omega/\omega \sim 10^{-6}$ [31], we eliminated the points that formed a peak wider than 10^{-5}. The candidate points were decreased to 7 by this line width veto.

The frequencies of remaining peaks are summarized in Table II. All the peaks were approximately multiples of 40 Hz. As you can see in Fig. 5, peaks in the error signal of the laser frequency control had the same frequency as the peaks that were not rejected in the veto process. As the axion signal should not be present in the error signal, this suggests that the cause of remaining candidate peaks are from mechanical resonances of the cavity. We therefore rejected all the remaining candidate peaks.

TABLE II. Summary of remaining peaks after the veto procedures.

Frequency (Hz)	SNR ρ (Measured value)	SNR ρ (Detection threshold)
81.6712	3243	109
119.983	2073	137
120.001	2616	137
120.113	1125	137
120.117	159	137
120.118	7637	137
396.142	373	313

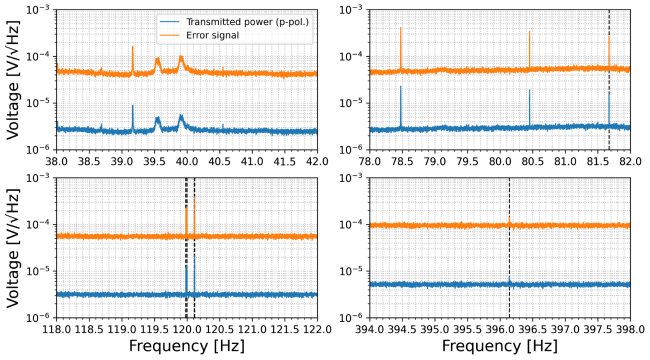

FIG. 5. The one-sided amplitude spectral density of the transmitted p-polarization signal (blue line) and the error signal (orange line) around 40 Hz (upper left panel), 80 Hz (upper right panel), 120 Hz (lower left panel), and 400 Hz (lower right panel). Black dashed lines are the frequencies corresponding to the 7 remaining peaks summarized in Table II.

We obtained the spectrum of the upper limit to the rotation angle of linearly polarized light $\delta\phi^{(\mathrm{upp})}(m_a)$ from the analysis pipeline, and calibrated it to the bound on the axion-photon coupling $g_{a\gamma\gamma}(m_a)$ from Eq. (19). Note that the upper bound on the rotation angle of linear polarization $\delta\phi^{(\mathrm{upp})}(m_a)$ and the response function $|H_a'|$ with the parameters of this work are plotted in the Appendix.

The initial value of $\delta\nu_{\mathrm{total}} = 2.52(2)$ MHz and the combination of $\delta\nu_1$ and $\delta\nu_2$ were found to be a major source of systematic effect, which will give 11% of difference in the upper limit at $m_a = 10^{-13}$ eV. The values of these parameters were chosen to set the most conservative upper limit. The results are shown in Fig. 6. The upper limit was limited by classical noises and worse than the current shot noise by 5 orders of magnitude. Since $\delta\nu_1$ and $\delta\nu_2$ were nonzero, the current shot noise sensitivity was worse than the design sensitivity in the low mass range and has the dip at $m_a \simeq 10^{-8}$ eV which corresponds to the frequency of $\delta\nu_{\mathrm{total}}$.

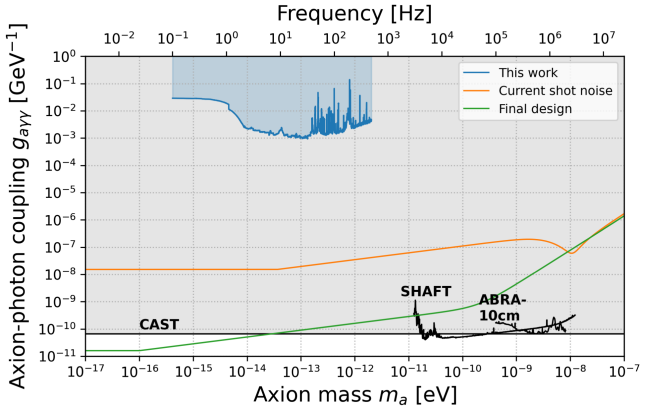

FIG. 6. The blue line shows the upper limit on the axion-photon coupling constant obtained by this work. We observed for $T_{\mathrm{obs}} = 86,400$ seconds. The orange line is the expected sensitivity limited by shot noise with the same parameters as this work assuming $T_{\mathrm{obs}} = 86,400$ seconds. The green line represents the designed shot noise limited sensitivity of DANCE Act-1 assuming a observation time of $T_{\mathrm{obs}} = 1$ year. The parameters which are used for this estimation are summarized in Table I. The black lines with the gray-shaded region are current bounds obtained from CAST [12], SHAFT [13], and ABRACADABRA-10 cm [14] experiments.

V. CAUSES OF SENSITIVITY DEGRADATION

We discuss the two causes of sensitivity degradation in this experiment here. One is classical noise sources and the other is a nonzero phase difference between the two polarizations.

The rotation angle of linear polarization in 0.1–1 Hz correlated significantly with the injected laser power, and the rotation angle of linear polarization in 30 Hz–5 kHz correlated with the error signal for the frequency control. Thus, laser intensity noise, laser frequency noise, and mechanical vibration are some of the candidates for noise sources limiting our sensitivity. Furthermore, in principle the phase noises such as laser frequency noise and mechanical vibration are not supposed to contribute to noise for DANCE, which observes the signal in amplitude quadrature, but it could have coupled in this demonstration. The reduction of these noise sources is underway in our upgraded setup to be reported in future work.

The sensitivity is also reduced because of the reflective phase difference between two linear polarizations. If we can realize $\delta\nu_1 = \delta\nu_2 = 0$, the sensitivity will improve by 3 orders of magnitude. We aim to deal with this issue by constructing an auxiliary cavity to achieve simultaneous resonance between both polarizations [19,34].

VI. CONCLUSION

The broadband axion DM search with a bow-tie cavity, DANCE Act-1 was demonstrated. We searched for the rotation and oscillation of linearly polarized light caused by the axion-photon coupling for 86,400 seconds and obtained the first results by DANCE. We found no evidence for axions and set 95% confidence level upper limit on the axion-photon coupling $g_{a\gamma\gamma} \lesssim 8 \times 10^{-4}$ GeV^{-1} in the axion mass range of 10^{-14} eV $< m_a < 10^{-13}$ eV.

The candidates for noise sources limiting our sensitivity are laser intensity noise, frequency noise, and mechanical vibration. The sensitivity will be improved by introducing laser intensity control and a vibration isolation system as well as upgrading the frequency control system. The difference of reflective phase shift between s- and p-polarizations is also the cause for the sensitivity degradation. We are installing an auxiliary cavity to realize simultaneous resonance between the two polarizations [34].

Although the upper limit did not exceed the current best limits, this optical cavity experiment is the first

demonstration of polarization-based axion dark matter search without any external magnetic field. By sufficiently upgrading the setup using the techniques mentioned above, we are expecting to improve the sensitivity by several orders of magnitude.

ACKNOWLEDGMENTS

We would like to thank Shigemi Otsuka and Togo Shimozawa for manufacturing the mechanical parts, Kentaro Komori and Satoru Takano for fruitful discussions, and Ching Pin Ooi for editing this paper. This work is supported by JSPS KAKENHI Grants No. JP18K13537, No. JP20H05850, No. JP20H05854, and No. JP20H05859, by the Sumitomo Foundation, and by JST PRESTO Grant No. JPMJPR200B. Y. O. is supported by Grant-in-Aid for JSPS Fellows No. JP22J21087 and by JSR Fellowship, the University of Tokyo. H. F. is supported by Grant-in-Aid for JSPS Fellows No. JP22J21530 and by Forefront Physics and Mathematics Program to Drive Transformation (FoPM), a World-leading Innovative Graduate Study (WINGS) Program, the University of Tokyo. J. K. is supported by Grant-in-Aid for JSPS Fellows No. JP20J21866 and by research program of the Leading Graduate Course for Frontiers of Mathematical Sciences and Physics (FMSP). A. N. is supported by JSPS KAKENHI Grants No. JP23K03408, No. JP23H00110, and No. JP23H04893. I. O. is supported by JSPS KAKENHI Grant No. JP19K14702.

APPENDIX: LIKELIHOOD FUNCTION OF SNR AND THE UPPER LIMITS

As shown in Ref. [28], the Fourier mode of signal with mass m_a can be expressed in terms of the stochastic variables as

$$\delta\phi(f_n;m_a) \simeq g_{a\gamma\gamma}(m_a)\frac{\sqrt{2\rho_a}}{2k_0}|H_a'(m_a)|T \times \sqrt{\Delta_s(f_n;m_a)}\left[\frac{r_n}{\sqrt{2}}e^{i\theta_n}\right], \tag{A1}$$

$$\equiv \delta\phi(m_a)\frac{T}{2}\sqrt{\Delta_s(f_n;m_a)}\left[\frac{r_n}{\sqrt{2}}e^{i\theta_n}\right], \tag{A2}$$

where θ_n and r_n respectively obey a uniform distribution over $[0,2\pi]$ and the standard Rayleigh distribution. $\Delta_s(f_n;m_a)$ is the analytic function that represents the deterministic part of the spectral shape determined by the velocity distribution of DM (see Ref. [28] for details). By performing the marginalization over r_n, the likelihood that takes into account the random amplitude of DM signal can be obtained as

$$\mathcal{L}(\rho_n|\lambda_n) \equiv \int \mathrm{d}r_n\, P_R(r_n)\mathcal{L}(\rho_n|\lambda_n r_n) = \frac{1}{2(1+\lambda_n^2)}\exp\left(\frac{-\rho_n}{2(1+\lambda_n^2)}\right), \tag{A3}$$

where $\rho_n = 4|\tilde{\phi}(f_n)|^2/TS(f_n)$ is the SNR at frequency bin f_n. As can be seen, the likelihood is characterized by the parameter

$$\lambda_n \equiv \delta\phi(m_a)\sqrt{\Delta_s(f_n;m_a)}\sqrt{\frac{T}{2S(f_n)}}, \tag{A4}$$

that depends on the characteristic amplitude of signal $\delta\phi(m_a)$. Then from this expression, the likelihood for the (total) SNR $\rho = \Sigma_n\rho_n$ defined in Eq. (17) can be derived as

$$\mathcal{L}(\rho|\{\lambda_n\}) = \int\left(\prod_l^{N_{\mathrm{bin}}}\mathrm{d}\rho_n\,\mathcal{L}(\rho_n|\lambda_n)\right)\delta\left(\rho-\sum_n^{N_{\mathrm{bin}}}\rho_n\right) = \sum_n^{N_{\mathrm{bin}}}\frac{w_n}{2(1+\lambda_n^2)}\exp\left(-\frac{\rho}{2(1+\lambda_n^2)}\right), \tag{A5}$$

$$w_n \equiv \prod_{n'(\neq n)}^{N_{\mathrm{bin}}}\frac{1+\lambda_n^2}{\lambda_n^2-\lambda_{n'}^2}, \tag{A6}$$

where $\lambda_n \neq \lambda_{n'}$ is assumed for all frequency bins $n \neq n'$. We should note that this assumption would be violated and there arises a numerical instability, specifically for higher DM masses which involves more frequency bins in Eq. (17). In this case, however, we can use the Gaussian approximation of Eq. (A5):

$$\mathcal{L}(\rho|\{\lambda_n\}) \to \frac{1}{\sqrt{2\pi\sigma_\rho^2}}\exp\left(-\frac{(\rho-\mu_\rho)^2}{2\sigma_\rho^2}\right) \quad \text{for } T \gg \tau, \tag{A7}$$

$$\mu_\rho = 2\sum_n(1+\lambda_n^2), \tag{A8}$$

$$\sigma_\rho^2 = 4\sum_n(1+\lambda_n^2)^2. \tag{A9}$$

In our analysis, we apply this Gaussian approximation for $N_{\mathrm{bin}} > 8$.

From these expressions of likelihood function, we could numerically set the 95% confidence limit on $\{\lambda_n\}$, or equivalently on $\delta\phi(m_a)$ according to Eq. (18). The upper bound $\delta\phi^{(\mathrm{upp})}(m_a)$ derived in our pipeline is shown in Fig. 7. As mentioned in the main text, $\delta\phi^{(\mathrm{upp})}(m_a)$ is converted to the upper limit on $g_{a\gamma\gamma}$ with Eq. (19). This was achieved by using the response function $|H_a'|$ presented in Fig. 8.

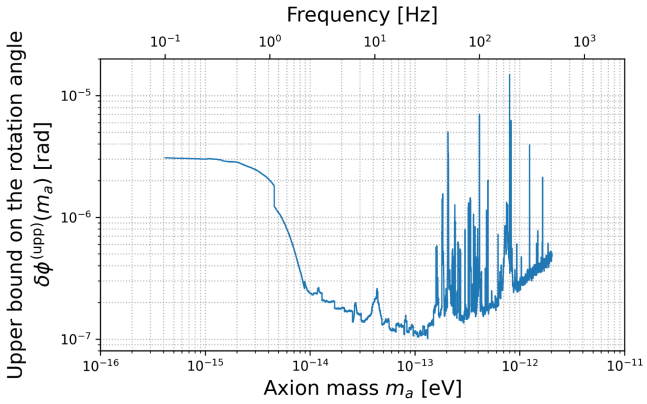

FIG. 7. The upper bound on the rotation angle of linear polarization $\delta\phi^{(\mathrm{upp})}(m_a)$.

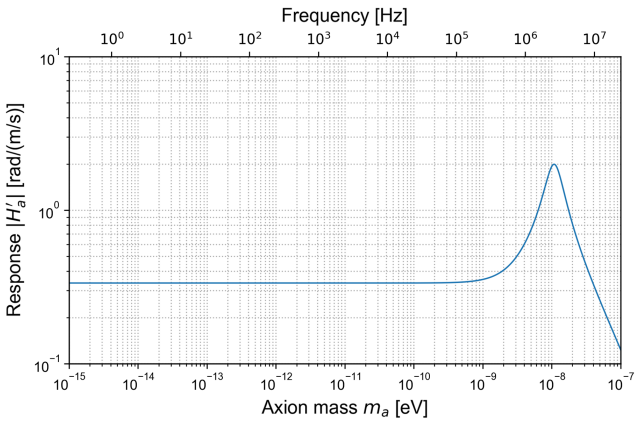

FIG. 8. The response function with the parameters of this experiment $|H'_a|$. The parameters were chosen from Table I to set the most conservative upper limit.

[1] R. D. Peccei and H. R. Quinn, Phys. Rev. Lett. **38**, 1440 (1977).
[2] A. Arvanitaki, S. Dimopoulos, S. Dubovsky, N. Kaloper, and J. March-Russell, Phys. Rev. D **81**, 123530 (2010).
[3] J. Preskill, M. B. Wise, and F. Wilczek, Phys. Lett. **120B**, 127 (1983).
[4] L. Abbott and P. Sikivie, Phys. Lett. **120B**, 133 (1983).
[5] M. Dine and W. Fischler, Phys. Lett. **120B**, 137 (1983).
[6] P. Arias, D. Cadamuro, M. Goodsell, J. Jaeckel, J. Redondo, and A. Ringwald, J. Cosmol. Astropart. Phys. 06 (2012) 013.
[7] P. Sikivie, Phys. Rev. Lett. **51**, 1415 (1983).
[8] M. B. Schneider, F. P. Calaprice, A. L. Hallin, D. W. MacArthur, and D. F. Schreiber, Phys. Rev. Lett. **52**, 695 (1984).
[9] G. Raffelt and L. Stodolsky, Phys. Rev. D **37**, 1237 (1988).
[10] A. Payez, C. Evoli, T. Fischer, M. Giannotti, A. Mirizzi, and A. Ringwald, J. Cosmol. Astropart. Phys. 02 (2015) 006.
[11] C. S. Reynolds, M. C. D. Marsh, H. R. Russell, A. C. Fabian, R. Smith, F. Tombesi, and S. Veilleux, Astrophys. J. **890**, 59 (2020).
[12] CAST Collaboration, Nat. Phys. **13**, 584 (2017).
[13] A. V. Gramolin, D. Aybas, D. Johnson, J. Adam, and A. O. Sushkov, Nat. Phys. **17**, 79 (2021).
[14] C. P. Salemi, J. W. Foster, J. L. Ouellet, A. Gavin, K. M. W. Pappas, S. Cheng, K. A. Richardson, R. Henning, Y. Kahn, R. Nguyen, N. L. Rodd, B. R. Safdi, and L. Winslow, Phys. Rev. Lett. **127**, 081801 (2021).
[15] A. C. Melissinos, Phys. Rev. Lett. **102**, 202001 (2009).
[16] W. DeRocco and A. Hook, Phys. Rev. D **98**, 035021 (2018).
[17] I. Obata, T. Fujita, and Y. Michimura, Phys. Rev. Lett. **121**, 161301 (2018).
[18] H. Liu, B. D. Elwood, M. Evans, and J. Thaler, Phys. Rev. D **100**, 023548 (2019).
[19] D. Martynov and H. Miao, Phys. Rev. D **101**, 095034 (2020).
[20] K. Nagano, T. Fujita, Y. Michimura, and I. Obata, Phys. Rev. Lett. **123**, 111301 (2019).
[21] K. Nagano, H. Nakatsuka, S. Morisaki, T. Fujita, Y. Michimura, and I. Obata, Phys. Rev. D **104**, 062008 (2021).
[22] Y. Michimura, Y. Oshima, T. Watanabe, T. Kawasaki, H. Takeda, M. Ando, K. Nagano, I. Obata, and T. Fujita, J. Phys. Conf. Ser. **1468**, 012032 (2020).
[23] Y. Oshima, H. Fujimoto, M. Ando, T. Fujita, Y. Michimura, K. Nagano, I. Obata, and T. Watanabe, arXiv:2105.06252.
[24] Y. Oshima, H. Fujimoto, M. Ando, T. Fujita, J. Kume, Y. Michimura, S. Morisaki, K. Nagano, H. Nakatsuka, A. Nishizawa, I. Obata, and T. Watanabe, J. Phys. Conf. Ser. **2156**, 012042 (2021).
[25] S. M. Carroll, G. B. Field, and R. Jackiw, Phys. Rev. D **41**, 1231 (1990).
[26] S. M. Carroll, Phys. Rev. Lett. **81**, 3067 (1998).
[27] H. Fujimoto, Y. Oshima, J. Kume, S. Morisaki, K. Nagano, T. Fujita, I. Obata, A. Nishizawa, Y. Michimura, and M. Ando (to be published).
[28] H. Nakatsuka, S. Morisaki, T. Fujita, J. Kume, Y. Michimura, K. Nagano, and I. Obata, arXiv:2205.02960.
[29] R. W. P. Drever, J. L. Hall, F. V. Kowalski, J. Hough, G. M. Ford, A. J. Munley, and H. Ward, Appl. Phys. B **31**, 97 (1983).
[30] H. Fujimoto, Y. Oshima, M. Ando, T. Fujita, Y. Michimura, K. Nagano, and I. Obata, arXiv:2105.08347.
[31] A. Derevianko, Phys. Rev. A **97**, 042506 (2018).
[32] G. Bertone, D. Hooper, and J. Silk, Phys. Rep. **405**, 279 (2005).
[33] N. W. Evans, C. A. J. O'Hare, and C. McCabe, Phys. Rev. D **99**, 023012 (2019).
[34] H. Fujimoto, Y. Oshima, M. Ando, T. Fujita, Y. Michimura, K. Nagano, and I. Obata, J. Phys. Conf. Ser. **2156**, 012182 (2021).

Correction: Equation (13) contained a minor error and has been fixed. The previously published Figs. 2 and 8 contained incorrect values on the y axes and have been replaced.